WASI-AI: Synergistic Integration of AI and Physics for Retrieving Water Quality and Benthic Parameters from Multi- and Hyperspectral Images

Milad Niroumand-Jadidi, *Member, IEEE*, and Peter Gege

***Abstract*—Artificial intelligence (AI) has spurred significant progress in the remote sensing of water constituents through physical models that rely on a predefined database of simulations, e.g., Case-2 Regional/Coast Color processor. However, these models are sensor-specific, not applicable in optically shallow waters, and incapable of adapting to different bio-optical conditions. This study introduces a novel approach that synergistically integrates AI with physics-based modeling. The developed method, termed water color simulator AI (WASI-AI), is implemented as a new module into the WASI software. WASI-AI uses the physics-based WASI two-dimensional (2-D) (WASI-2D) module of WASI to retrieve the unknown biophysical parameters for a small subset of image pixels selected at random. A portion of the inverted samples is used to train neural networks (NNs). The trained NNs are then applied to predict the unknown biophysical parameters for all water pixels of the image. The remaining portion of the samples is used to assess the agreement between WASI-AI and WASI-2D retrievals. WASI-AI maintains the advantages of WASI-2D regarding sensor independence and flexibility in bio-optical adaptation. The correlation plots of WASI-AI versus WASI-2D allow recognizing spectral ambiguity and optimizing inverse modeling parametrization. The integration of AI significantly speeds up the inversion, reducing the processing time of a single image from hours/days to mere minutes. We applied WASI-AI to hyperspectral (EnMAP, DESIS) and multispectral (Sentinel-2, Landsat-8/9, Planet SuperDove) imagery in optically deep and shallow waters. After handling spectral ambiguities, the results indicate a strong correspondence between WASI-AI and WASI-2D inversions, with WASI-AI exhibiting lower noises on the maps.**

***Index Terms*—Aquatic remote sensing, artificial intelligence, bathymetry, benthic properties, model integration, physics-based inversion, spectral ambiguities, water color simulator (WASI), WASI-AI, water quality.**

I. Introduction

THE monitoring of water quality parameters and benthic properties (e.g., bathymetry and substrate types) by means of optical remote sensing supports a wide range of aquatic science and management applications concerned with ecosystem function and services as well as environmental conservation [1], [2]. The development of methods for spectrally-based retrieval of biophysical parameters in aquatic environments has undergone significant progress over the past decades. The methodological development has mainly been aligned with the advancement of satellite sensors [3], [4]. Initial efforts were mainly focused on algorithm development for ocean color sensors with coarse spatial resolutions, e.g., SeaWiFS with a spatial resolution of 4 km. The spatial resolution of these sensors is mainly suitable for studying oceanic and open waters, where the chlorophyll-a (Chl-a) concentration dominates the optical properties [5]. The launches of Landsat-8 and Sentinel-2 marked a significant turning point in monitoring inland and nearshore coastal waters, given their suitable spatial (10−30 m) and radiometric (12 bit) resolutions [4], [6]. The latest Landsat-9 satellite has showcased an improved capability for bathymetry and water quality retrieval, which can be attributed to the enhanced radiometric quantization of 14 bit [7], [8]. In optically complex waters, besides Chl-a, other constituents like total suspended matter (TSM) and colored dissolved organic matter (CDOM) can remarkably impact water-leaving radiance [9]. Moreover, the bottom-reflected radiance in optically shallow waters further complicates the estimation of constituents [10]. Given that various factors impact the water-leaving signal in optically complex waters, the spectral ambiguity problem becomes more severe [11], posing a major challenge to algorithm development. The spectral ambiguity problem can be partially mitigated using hyperspectral data with an adequate signal-to-noise ratio (SNR) [3], [12], [13]. There is a recent growth in the availability of hyperspectral satellite images at 30 m spatial resolution, particularly from Precursore IperSpettrale della Missione Applicativa (PRISMA), DLR earth sensing imaging spectrometer (DESIS), and environmental mapping and analysis program (EnMAP) missions that have attracted the attention of aquatic remote sensing community in retrieving water constituents [14], [15].

Various methods are available for retrieving biophysical parameters in aquatic systems that fall into the two main categories of empirical and physics-based models [3], [4]. The empirical approaches involve creating a statistical relationship between spectra-derived features (e.g., single bands or ratios) and colocated field-measured values of the parameter of interest [3], [16]. Previous studies have employed different types of regression for empirical modeling, including polynomials and newer artificial

Received 30 September 2024; revised 15 March 2025 and 22 June 2025; accepted 23 August 2025. Date of publication 1 September 2025; date of current version 15 September 2025. *(Corresponding author: Milad Niroumand-Jadidi.)*

Milad Niroumand-Jadidi is with the Interdepartmental Research Center for Environmental Sciences, University of Bologna, 48121 Ravenna, Italy (e-mail: milad.niroumand@unibo.it).

Peter Gege is with the Remote Sensing Technology Institute, German Aerospace Center (DLR), D-82234 Weßling, Germany (e-mail: peter.gege@dlr.de).

Digital Object Identifier 10.1109/JSTARS.2025.3605061

intelligence (AI) models [3], [17]. The literature presents some pure data-driven approaches for water quality retrieval using deep learning, which are suitable for large training sets or long time-series analyses [18], [19], [20], [21]. Unlike purely data-driven empirical approaches, physical models account for the interaction of light with the atmosphere, water surface, water body, and benthic substrate (in optically shallow waters) at different portions of the spectrum [22]. The physics-based techniques invert a radiative transfer model that accounts for the absorption and backscattering properties of the different media that the light interacts with [23]. The inversion is based either on look-up tables (LUTs) or analytical models. The LUT-based approaches employ a predefined set of radiative transfer simulations to seek a simulated spectrum optimally matching the observed spectrum (e.g., using a least-squares minimization) in terms of shape and magnitude [24]. Another approach based on LUTs relies on training neural networks (NNs) using the predefined dataset of simulations, e.g., Case-2 Regional/Coast Color (C2RCC) processor [25]. The LUT-based techniques are sensor-specific; i.e., the spectral simulations make use of the spectral response of a given sensor when creating the database. In contrast, the analytical approaches do not involve a predefined set of simulations and allow for greater flexibility in the parametrization of the forward model to generate the simulated spectra. These techniques perform the simulations in a user-defined range of specific inherent optical properties (SIOPs) and simultaneously seek the optimal match with the observed spectrum [26]. The inversion can be adapted easily and quickly to any sensor and bio-optical condition. Both empirical and physics-based approaches have their pros and cons, summarized as follows.

1) The empirical approaches are straightforward in terms of implementation, with no need for a detailed understanding of the underlying physics, and the image processing is fast. However, they require a considerable number of in situ measurements to train the regression model effectively. The field measurements need to be acquired simultaneous to the image acquisition and represent the variability of bio-optical conditions within the water body. Thus, the empirical models are image-specific and have severe limitations in terms of spatiotemporal transferability [27].
2) The LUT-based physical models are trained for certain water types and a specific sensor, which makes them computationally fast. However, they cannot be adapted by the user to site-specific concentration ranges or IOPs which, together with the sensor dependency, limits their application. Furthermore, to our knowledge all currently available LUT-based models, including those based on AI inversion like C2RCC [25], are developed for optically deep waters and cannot be used for retrieving benthic information.
3) The analytical model approaches are flexible in defining the optical properties of water constituents and bottom substrates, restricting the parameter ranges and handling sensor properties. Publicly available software tools are the two-dimensional (2-D) module of the WASI [26], [28] and the bio-optical model based tool for estimating water quality and bottom properties from remote sensing images, BOMBER [29]. The user can adapt the inversion to any bio-optical condition in optically deep or shallow waters. As the center wavelengths and bandwidths of the simulated spectra are automatically adjusted to those of the sensor of interest, these models can be applied to any multispectral and hyperspectral image acquired from spaceborne, airborne, and drone platforms. However, a major drawback of analytical model inversion is its computational cost. This approach performs a complete physical model inversion for each pixel, requiring numerous iterations to find an optimal match between the pixel spectrum and the simulations. This process can be extremely time-consuming when applied to large water bodies. For instance, processing a single Sentinel-2 image (20 m resolution) for a lake the size of Garda (Italy) can take $\sim$20 h using the WASI-2D software. Therefore, analytical model inversion techniques are not well-suited for routine image processing.

AI has so far been utilized in two main ways in retrieving aquatic biophysical parameters: 1) through empirical regression, which lacks physical concepts and is limited by the availability of in situ data, and 2) through physics-based models such as C2RCC, which employs AI to train models using precalculated LUTs. The sensor-dependency and lack of flexibility in bio-optical adaptation are discussed above as key drawbacks of the latter approach. Although this approach does involve some integration of AI and physics, AI plays a role only after creating the database of simulations, and it does not provide any support for the parametrization of physical models. Synergistic integration of AI and physics-based models is now a vital next step to exploit further the benefits of the two fields.

This study introduces a novel approach that seamlessly merges AI with physical models. The new model uses physics-based inversions to train AI and also utilizes AI to optimize the parametrization of physical models, establishing a two-way learning process (from physics to AI and vice versa). The developed approach, termed WASI-AI, first performs an analytical inversion of a small number of image pixels using WASI-2D with a user-defined choice of the retrieval (fit) parameters and associated SIOPs and initial values. Then, a portion of the samples inverted by WASI-2D is used to train NNs for each fit parameter. The trained models are then used to predict the fit parameters for all water pixels. The portion of samples not seen through training is then used to assess the agreement between WASI-2D and WASI-AI retrievals. As the inversion methodologies of WASI-2D and WASI-AI are independent, the agreement analysis provides feedback on the suitability of parametrization used for the physical models that can guide the user to optimize the inversion. This synergistic AI and physics integration through WASI-AI pursues the following objectives: 1) integration of AI with the physics-based WASI-2D while maintaining flexibility in adapting to any bio-optical condition and being sensor-independent. The AI integration aims to provide feedback on the parametrization of physical models and significantly speed up the inversion; 2) implementation of WASI-AI as a freely available software module to the public; 3) application of WASI-AI on a comprehensive set of multi- and hyperspectral imagery acquired over various water bodies

with diverse bio-optical conditions. The WASI-AI retrievals are rigorously assessed by performing agreement analysis relative to the standard WASI-2D inversion results. Furthermore, the noise levels are quantified for the maps derived from both methods.

The rest of this article is organized as follows. Section II briefly describes the WASI software along with its 2-D module and then elaborates on the developed WASI-AI and assessment metrics. Section III outlines the image dataset used in the study. Section IV provides WASI-2D and WASI-AI inversion results and the agreement analysis between the two models. Section V provides discussion. Finally, Section VI concludes this article.

II. Methods

A. WASI-2D: Inversion Based on Physical Models

WASI is a well-established and publicly available software tool for the simulation and analysis of different types of spectral measurements in deep and shallow waters. It is based on a number of physical models that parameterize the illumination-dependent apparent optical properties and light field parameters of water bodies in terms of analytical equations, which make use of wavelength-dependent material-specific, so-called SIOPs and parameters describing the environmental and illumination conditions such as concentrations of water constituents, water depth, areal fractions of benthic cover types, sun zenith angle, and viewing angle. WASI can be adapted to any bio-optical condition in optically deep and shallow waters by changing the parameters or spectra defining the SIOPs of water constituents and the albedo of bottom substrates. A representative database is provided together with WASI, but the user can easily exchange each spectrum with a site-specific measurement. The details of WASI are provided in [28] and [30].

The WASI module WASI-2D allows the inversion of multispectral and hyperspectral images corrected for atmospheric effects [26]. The inversion iteratively simulates spectral measurements and systematically changes the values of certain model parameters (called fit parameters) until the simulated spectrum agrees with the measured spectrum as well as possible. The agreement between the two spectra is quantified by the residual, which is, by default, the sum of squared differences (least squares) but can be changed by the user, for example, by weighting each spectrum band individually. WASI-2D has been used in various studies, e.g., [14], [31], [32], [33], [34].

The diversity and different compositions of SIOPs introduce a fundamental numerical problem to inversion: different combinations of water constituents can lead to indistinguishable reflectance spectra [11]. This problem, known as spectral ambiguity, cannot be generally solved. However, it can be handled by restricting the variability of SIOPs to the relevant ones, analyzing correlations between parameters, or limiting the ranges of the variable parameters. All these measures require site-specific knowledge and are difficult to implement in software to process global data sets. WASI-2D is designed to handle these spectral ambiguities by allowing the user to import site-specific SIOPs, deciding for all model parameters if they shall be used as fit parameters or kept constant, assigning appropriate values to each model parameter, and defining image-specific initial values and ranges for each fit parameter. WASI-2D provides reasonable defaults for all settings, so the adjustment to a certain image usually requires only changing a few default values. Table III in [26] lists all parameters, which can potentially be used as fit parameters in WASI-2D and suggests, which to fit and which to keep constant for different conditions. The fit parameters relevant to this study are summarized in Table I.

TABLE I
Fit Parameters of WASI-2D Used in This Study

Symbol	Unit	Description
C_i	mg m^{-3}	Concentration of phytoplankton class i in terms of Chl-a. Name of phytoplankton group is used as a subscript (e.g., $C_{diatoms}$)
C_X	g m^{-3}	Concentration of TSM
C_Y	m^{-1}	Concentration of CDOM in terms of absorption at 440 nm
z_B	m	Water depth
$f_{A,i}$	-	Areal fraction of bottom substrate type number i
g_{dd}	sr^{-1}	Fraction of sky radiance due to direct solar radiation (sun glint)

B. WASI-AI: Inversion Based on AI and Physics Integration

The newly developed method WASI-AI synergistically incorporates AI into the inversion process of WASI-2D to identify ambiguity problems, assist the user in tuning the fit and fixed parameters and ranges of the physical models, and significantly reduce computational time. The concept of WASI-AI is to invert only a small number (in the order of several hundred) of image pixels, selected at random, based on the analytical models implemented in WASI-2D. Then, WASI-AI refines the inverted samples by identifying and eliminating outliers. The outliers are defined as samples with WASI-2D residuals higher than three scaled median absolute deviations from the median [35].

The refined samples serve as training and validation sets for NN regression models. The latter is a holdout portion of the inverted samples not seen through the training. Among different AI models, we rely on NNs as they are proven to be powerful in learning complex and nonlinear relations between the input features (spectral data) and the response (fit) parameter [36]. The NNs in WASI-AI comprise feedforward fully connected layers, and the layer size is automatically chosen depending on the number of spectral bands. Specifically, two fully connected layers are considered for multispectral imagery (< 20 bands), whereas four layers are used for hyperspectral images. Deeper networks with more layers are unsuitable since our objective is to limit the training set to a few hundred pixels, suiting well for shallow networks. The NNs for hyperspectral images involve more layers to handle the complexity of the data. The spectra of training samples feed the first fully connected layer as input to the NN. The input to each fully connected layer is multiplied by a weight matrix, followed by adding a bias vector [36]. The network response is a fit parameter whose values for the training set are known from WASI-2D inversion. The working mechanism of such NNs is extensively described in the literature [36], [37]. WASI-AI trains an individual NN for each fit parameter, and these NNs are subsequently used to predict the fit parameters for all water pixels. Since WASI-AI is designed for image-specific inversion (training and prediction

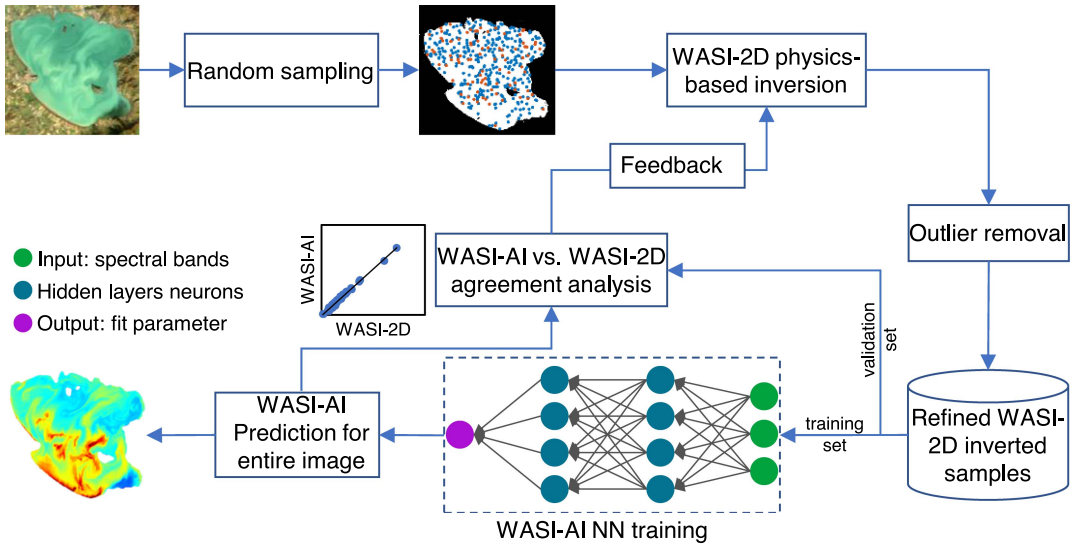

Fig. 1. Workflow of the developed WASI-AI that integrates NN-based image processing into the physics-based inversion of WASI-2D. Arbitrary numbers of layers and neurons are shown in the NN architecture for illustration.

on the same image), the likelihood of overfitting is minimal, as the model is not intended to transfer to other datasets. Moreover, as the training data are randomly selected from various locations on the image, they effectively capture the variability of the fit parameters. Consequently, the trained NNs rarely encounter predictions outside the range of training data.

The WASI-AI estimates for the validation samples are then regressed against WASI-2D fit results, and agreement metrics (see Section II-C) are computed. The WASI-AI vs. WASI-2D plots provide an effective means of assessing the suitability of WASI-2D parametrization and identifying ambiguity problems. Since the WASI-2D and WASI-AI inversions are based on independent approaches, a poor correspondence between their inversion results demonstrates that the solution of the inversion problem is ambiguous, whereas a strong agreement shows that the results are independent of the retrieval algorithm and the parameter can be derived reliably from the available spectral information with the chosen model parameterization. The agreement analysis, therefore, provides valuable feedback to the user, allowing to tune the physical modeling and repeat the inversion if needed. Therefore, WASI-AI not only preserves the flexibility of WASI-2D in adapting to diverse sensors and bio-optical conditions but also contributes to improving the parametrization of physical models, ultimately enhancing the quality of inversion.

The conventional WASI-2D image processing module performs inverse modeling for every pixel individually, which is time-demanding. The processing time of a single image can range from several hours to days, depending on the size of the water body and the number of pixels. This computationally demanding inversion process makes WASI-2D and similar physics-based processors less favorable for routine image processing. Furthermore, the problem of processing time can be exacerbated when spectral ambiguities make it necessary to tune the parametrization and repeat the inversion process. In contrast, WASI-AI uses the WASI-2D inversion for only hundreds of pixels through the training phase. Then, the NNs perform the entire image analysis, speeding up the process significantly.

The new method has been seamlessly integrated into WASI as module WASI-AI, making it readily accessible to the public (details in the Software Availability section). The workflow of the developed WASI-AI is illustrated in Fig. 1.

C. Agreement Analysis

As mentioned in Section II-B, WASI-AI assesses the agreement between estimates of WASI-AI and WASI-2D for the validation samples. We use a set of metrics for the agreement analysis, including the coefficient of determination (R^2), root-mean-square difference (RMSD), normalized RMSD (NRMSD) expressed in percentage, and bias [38]. The following equations define the metrics:

$$R^2 = \frac{\sum_{i=1}^{n}\left(E_i^{AI} - \overline{E^{2D}}\right)^2}{\sum_{i=1}^{n}\left(E_i^{2D} - \overline{E^{2D}}\right)^2}, \quad \overline{E^{2D}} = \frac{1}{n}\sum_{i=1}^{n} E_i^{2D} \tag{1}$$

$$\text{RMSD} = \left(\frac{\sum_{i=1}^{n}\left(E_i^{AI} - E_i^{2D}\right)^2}{n}\right)^{1/2} \tag{2}$$

$$\text{NRMSD} = \frac{\text{RMSD}}{\max\left(E^{2D}\right) - \min\left(E^{2D}\right)} \tag{3}$$

$$bias = 10^{\frac{\sum_{i=1}^{n}\log_{10}\left(E_i^{AI}/E_i^{2D}\right)}{n}} \tag{4}$$

E^{2D} and E^{AI} are the estimated values of a given fit parameter based on WASI-2D and WASI-AI, respectively, and n represents the number of samples. Note that $bias$ is calculated in a log-transformed space [38], and WASI-2D results are considered the reference. $bias$ values close to 1 imply that WASI-AI estimates are minimally biased with respect to the WASI-2D results.

TABLE II
STUDY SITES AND IMAGE DATA USED TO ASSESS THE PERFORMANCE OF WASI-AI RELATIVE TO WASI-2D

Water body	Surface (km^2)	Water type	Image	Acquisition date	Pixel size [m]	# Bands	Atmospheric correction	Fit parameters
Amathus Harbour (Cyprus)	13	Shallow	DESIS	9 Jun 2020	30	157	PACO	$z_B, f_{A,sand}, g_{dd}$
Lake Constance (Germany)	536	Deep	EnMAP	1 Aug 2022	30	73	PACO	$C_{green\ algae}, C_{diatoms}$ C_X, g_{dd}
		Deep	DESIS	14 Aug 2021	30	114	PACO	C_X, C_Y, g_{dd}
		Deep	Landsat-9	2 Aug 2022	30	6	ACOLITE	$C_{green\ algae}, C_X, g_{dd}$
		Deep	Sentinel-2	2 Aug 2022	20	9	ACOLITE	$C_{green\ algae}, C_X, g_{dd}$
Lake Garda (Italy)	370	Deep	Sentinel-2	17 Aug 2016	20	8	C2RCC	C_X, C_Y, g_{dd}
Lake Junin (Peru)	120	Deep & shallow	Landsat-8	8 Jul 2021	30	6	ACOLITE	Deep: C_X, C_Y, g_{dd} Shallow: $z_B, f_{A,silt}, f_{A,macrophytes}, g_{dd}$
		Deep & shallow	Sentinel-2	14 Jul 2021	20	9	ACOLITE	
Laguna Lasuntay (Peru)	0.2	Deep	SuperDove	16 Aug 2022	3	8	ACOLITE	$C_{green\ algae}, C_X, g_{dd}$
Lake Limassol (Cyprus)	11	Shallow	DESIS	9 Jun 2020	30	177	PACO	$z_B, f_{A,sand}, f_{A,macrophytes}$
Lake Trasimeno (Italy)	128	Deep	Sentinel-2	5 Jul 2019	20	8	C2RCC	$C_{green\ algae}, C_X, g_{dd}$

$bias > 1$ and $bias < 1$, respectively, convey overestimation and underestimation of WASI-AI estimates compared to WASI-2D. For instance, a $bias$ of 1.05 means that WASI-AI results are 5% overestimated relative to WASI-2D.

In addition to performing the agreement analysis for the validation samples, we perform a similar analysis for all image pixels. Thus, the entire image is inverted both with WASI-AI and WASI-2D. The results of fit parameters from the two methods are compared pixel by pixel, and the consistency metrics are calculated (1)–(4). The comparison suits well for quantifying the agreement between WASI-AI and WASI-2D but cannot identify systematic errors of the retrieved parameters, which may be caused, for example, by errors of atmospheric correction or the used SIOPs. Note that the goal of WASI-AI is not to improve the accuracy of WASI-2D but to identify spectral ambiguity problems and facilitate optimizing inverse modeling parametrization. Strong agreements between the inversion results of WASI-2D and WASI-AI indicate an appropriate handling of the spectral ambiguity problem using the WASI-AI vs. WASI-2D correlation plots. Therefore, the agreement analysis is independent of in situ data.

To facilitate the comparative analysis, difference maps (WASI-AI – WASI-2D) are produced and visualized through histograms. The noise level of map products is quantified using the coefficient of variation (CV), calculated as the ratio between the standard deviation and the mean of pixel values within sliding windows of 5×5. The CV maps are then averaged to compute the relative CV (RCV) as $CV^{\text{WASI-AI}}/CV^{\text{WASI-2D}}$. An RCV <1 indicates lower noise of the WASI-AI map than that of WASI-2D on average. The CV metric is also used to demonstrate the effectiveness of WASI-AI in addressing the ambiguity issue. We also compare the processing time of WASI-AI relative to WASI-2D by processing the entire image.

III. IMAGE DATASET

We use a comprehensive image dataset to evaluate the performance of WASI-AI relative to WASI-2D. The sensors have different spectral and spatial resolutions, and the water bodies cover a wide range of bio-optical conditions. The images are acquired with hyperspectral (EnMAP, DESIS) and multispectral (Landsat-8, Landsat-9, Sentinel-2, SuperDove) satellite sensors (see Table II). The images are processed with different atmospheric correction methods, including PACO [39], ACOLITE [40], and C2RCC [25]. The selection of atmospheric correction methods is based on the suitability of each processor for various sensors and water types. However, the methodology discussed in this study is not tied to any specific atmospheric correction approach. The case studies represent both optically deep and shallow waters. In the case of Lake Junin, different models and fit parameters are used for the optically deep and shallow parts of the lake (see Table II).

IV. RESULTS

In this section, we first describe how WASI-AI allows optimizing the parametrization of physical models to mitigate errors introduced by spectral ambiguities. The results of WASI-AI vs. WASI-2D agreement analysis after optimizing the inverse modeling are provided for all the images in Section IV-B. The following sections analyze WASI-AI's effectiveness in noise reduction and inversion acceleration.

A. Optimization of Inverse Modeling

As outlined in Section II-A, inverse modeling faces a significant challenge known as spectral ambiguities [11]. Although WASI-2D has been designed to handle this issue, it is not

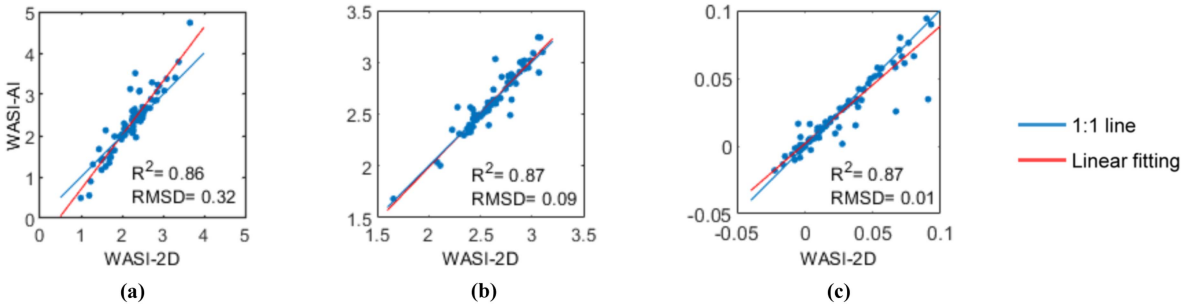

Fig. 2. Typical correlation plots created by WASI-AI, obtained for the Landsat-9 image of Lake Constance. These plots illustrate the correspondence between WASI-AI and WASI-2D for all fit parameters using validation samples, including (a) $C_{\text{green algae}}$ [mg/m^3], (b) TSM [g/m^3], and (c) g_{dd} [1/sr]. The plots specify R^2 and RMSD and are the basis for minimizing errors caused by spectral ambiguities.

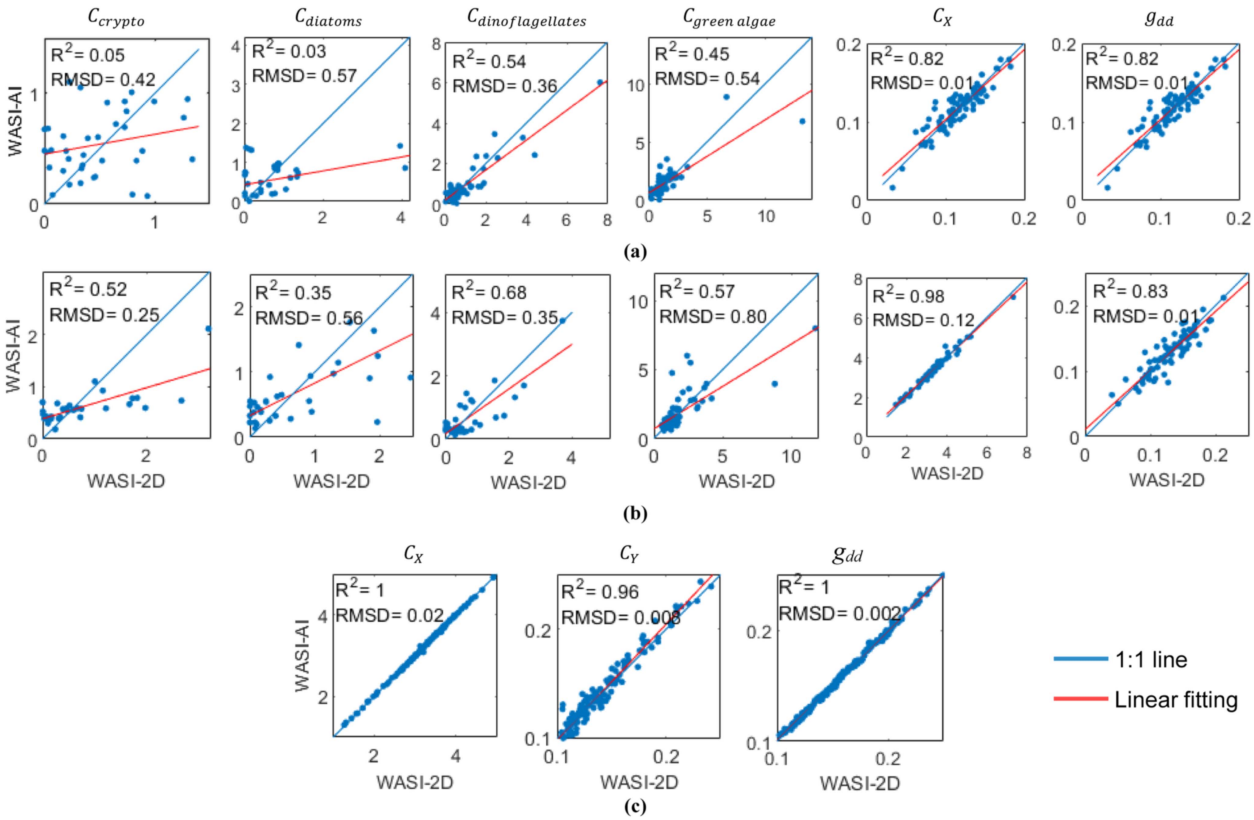

Fig. 3. Illustration of using correlation plots for handling the ambiguity problem at the example of phytoplankton classification from a DESIS image of Lake Constance. Row (a): six fit parameters (four C_i's, C_X, and g_{dd} from left to right) having all bands weighted equally. Row (b): same six fit parameters with spectral weighting applied. Row (c): three fit parameters (C_X, C_Y, g_{dd} from left to right) having all bands weighted equally without phytoplankton classification.

capable of detecting errors of fit results caused by these ambiguities. Introducing the new WASI-AI addresses this limitation by enabling the detection and quantification of errors caused by spectral ambiguities. This is achieved by processing the validation samples twice using entirely different methods. When fit parameters are sensitive to errors in other fit parameters (error propagation) or noise in the input data, changing the inversion method yields noticeable statistical differences in the fit results. In the absence of ambiguity problems, both methods produce similar results for validation samples due to WASI-AI being trained on the output of WASI-2D. However, when strong ambiguities are present, the results become decorrelated. Therefore, the correlation plots of WASI-AI versus WASI-2D, using the R^2 metric, prove effective in identifying these issues. Additionally, the average error caused by spectral ambiguities can be quantified using the RMSD metric. Fig. 2 presents an example of the correlation plots typical for the images processed in this study.

WASI-AI automatically generates the correlation plots, which quantify the correspondence between WASI-AI and WASI-2D results for the validation samples. These plots serve to identify fit parameters that cannot be reliably determined under the current settings. Based on these correlation plots, the impact of spectral ambiguities can be minimized by the user by systematically

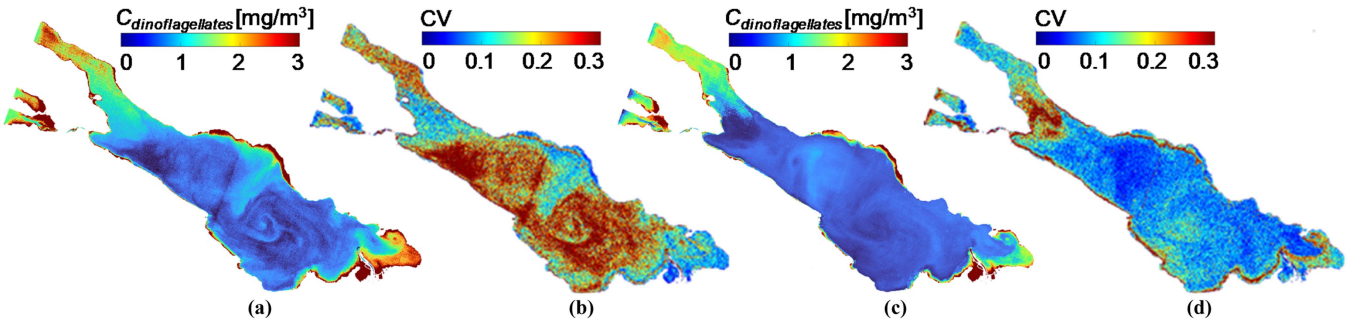

Fig. 4. Retrieval of dinoflagellates concentration from a DESIS image of Lake Constance and quantification of the retrieval noise expressed as the coefficient of variation (CV) before (a), (b) and after (c), (d) handeling the ambiguity issue by applying a spectral weighting function.

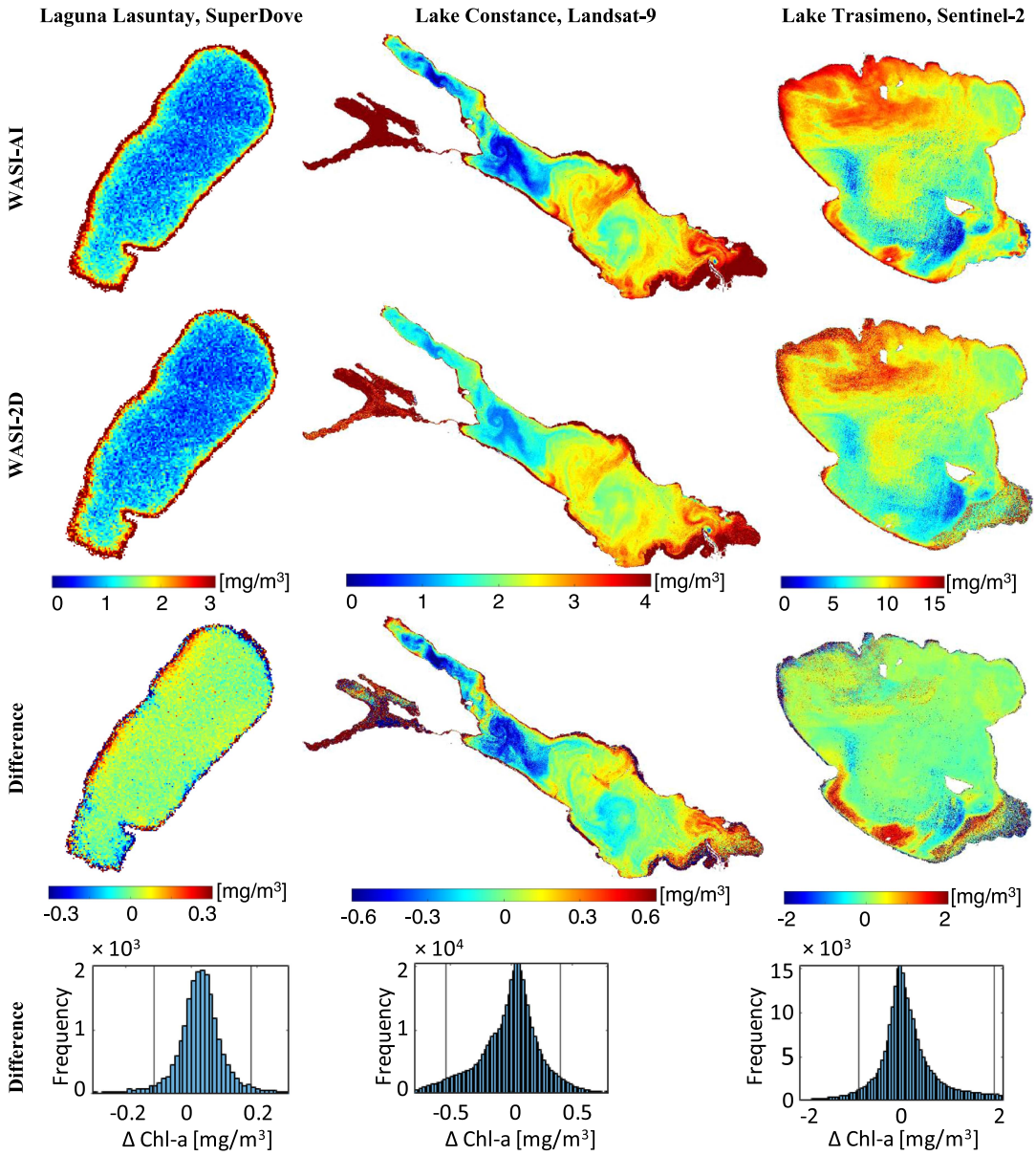

Fig. 5. Chl-a maps derived from WASI-AI and WASI-2D, along with associated difference maps and histograms.

TABLE III
AGREEMENT BETWEEN WASI-AI AND WASI-2D RESULTS

		C_{chl-a}	C_X	C_Y	z_B	f_A	g_{dd}
Parameter	Range	0.07-14 mg/m^3	0.1-15 g/m^3	0.01-1.1 m^{-1}	0.01-12 m	0-4.8	-1-0.92 sr^{-1}
	Mean	3.1 mg/m^3	2.4 g/m^3	0.24 m^{-1}	0.9 m	0.99	0.09 sr^{-1}
	SD	2.9 mg/m^3	1.7 g/m^3	0.23 m^{-1}	2.4 m	0.87	0.18 sr^{-1}
R²	Range	0.82-0.93 0.76-0.92	0.82-1 0.90-0.99	0.96-0.98 0.92-0.97	0.93-0.98 0.91-0.98	0.89-0.98 0.89-0.99	0.86-1 0.82-1
	Mean	0.87 0.85	0.95 0.94	0.97 0.95	0.95 0.94	0.94 0.95	0.95 0.94
	SD	0.03 0.05	0.06 0.03	0.01 0.02	0.02 0.03	0.04 0.04	0.05 0.06
NRMSD [%]	Range	5.6-10 4.9-7	1.1-6 0.5-5.9	1.4-3.3 1.6-3.4	2-5.4 1.9-4.8	1.8-6.1 1.7-4.1	0.5-5.9 0.5-5.9
	Mean	7.2 5.9	2.9 2.7	2.6 2.6	3.9 3.7	3.6 3.3	2.9 2.6
	SD	1.5 0.9	1.8 1.7	0.9 0.8	1.4 1.2	1.4 1	2.2 1.5
Bias	Range	0.98-1.04 0.97-1.06	0.99-1.01 1-1.07	1-1.01 0.97-1.02	1-1.05 1-1.04	0.95-1.06 0.98-1.05	0.87-1.03 0.89-1.03
	Mean	1 1.02	1 1.02	1 1	1.02 1.01	1 1	0.98 0.98
	SD	0.02 0.03	0.01 0.02	0.01 0.02	0.02 0.02	0.03 0.02	0.04 0.05

For each metric, the first value is associated with the validation holdout and the latter with the entire image.

adjusting the fit settings until a reasonable correlation is achieved for all fit parameters. Fig. 3 shows the correlation plots from two attempts to separate phytoplankton groups (PGs) using the hyperspectral DESIS image of Lake Constance. Using C_i of four PGs, C_X and g_{dd} as fit parameters, with equal weighting of all bands, the concentrations of two PGs are uncorrelated ($R^2<$ 0.1), indicating that only two PGs can be distinguished under the chosen fit settings [see Fig. 3(a)]. However, by employing a spectral weighting function adjusted to sensor noise and the spectrally dependent information content for PGs [41], the concentrations of all four PGs show at least a modest correlation ($R^2>0.35$). Consequently, PG classification could be enhanced, and the uncertainties arising from spectral ambiguities can be quantified [see Fig. 3(b)]. When only three parameters (C_X, C_Y, g_{dd}) are treated as fit parameters without attempting phytoplankton classification, the correlation of all parameters significantly increases [see Fig. 3(c)]. This is expected since reducing the number of variable parameters effectively minimizes the occurrence of spectral ambiguities. Hence, limiting the number of fit parameters is the most effective approach to mitigate the ambiguity problem. However, this strategy might hinder the detection of relevant parameters for specific applications. In the example of Fig. 3, configuring data processing for deriving maps of four PGs might be more interesting than optimizing all correlation plots. Even though some correlations are weak and the concentration uncertainties relatively large in Fig. 3(b), the PG maps, as shown in [41], still hold value, mainly because the RMSD in the correlation plots enables the quantification of their uncertainties. To highlight the advantage of WASI-AI in addressing the ambiguity issue, Fig. 4 presents the dinoflagellate maps before and after applying the spectral weighting function. Corresponding CV maps are included to quantify the noise levels in each case. Evidently, the noise level is significantly reduced after resolving the ambiguity issue, with the average CV decreasing by a factor of approximately 3. For brevity, maps are shown for one PG, but the average CV reduction across all PGs is about 5 times.

B. Agreement of WASI-AI and WASI-2D

Each image listed in Table II is processed twice, once using WASI-2D and once using WASI-AI. The random sampling of WASI-AI was set to 400 pixels within each image, from which 80% is used for training and the remaining for validation. Table III summarizes the agreement statistics for each fit parameter, both for the validation samples and the entire water pixels. The range, mean, and standard deviation (SD) values for each agreement metric are calculated as averages over all images. The results show that WASI-AI retrievals exhibit strong agreement with those of WASI-2D for both optically deep and shallow inversions. The typical R^2 is 0.95 for all fit parameters and NRMSD $<$ 3.9%, except for Chl-a, which has a slightly lower agreement ($R^2 = 0.85$, NRMSD $= 5.9\%$). The bias values for all fit parameters are close to one, indicating minimal systematic differences between the retrievals of the two methods. The agreement statistics for the entire image are comparable with those for validation samples, indicating that WASI-AI provides a robust inversion employing a few hundred image pixels as training data, and the statistical parameters derived from the validation samples are representative of the entire image. In addition to the complete agreement statistics (see Table III), we illustrate the results of WASI-AI and WASI-2D by comparing several maps for each fit parameter (see Figs. 5–9). The difference maps and associated histograms are also provided for better visual comprehension of the agreements between the maps of the two methods. While it is not feasible to show all

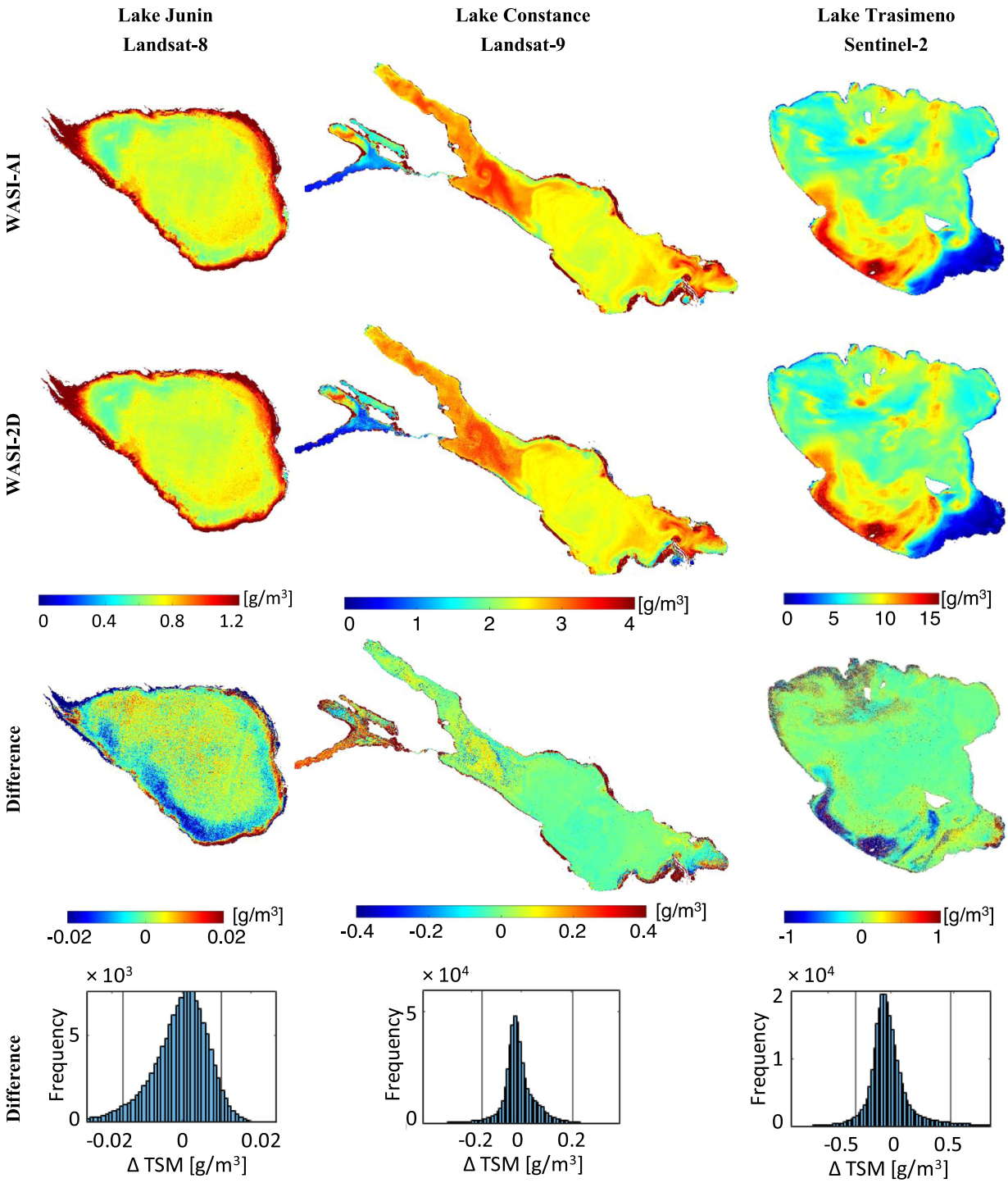

Fig. 6. TSM maps derived from WASI-AI and WASI-2D, along with associated difference maps and histograms.

the maps due to their large number, we provide representative examples for each fit parameter associated with different water bodies and images. In optically deep waters, the nearshore areas with possible interferences on the R_{rs} data due to the bottom effects are excluded from the computation of the agreement statistics (see Table III). However, we visualize these areas on the maps to gain insights into the relative performance of the two methods for the areas where the parametrization of physical models is unsuited. For example, in the shallow region on the western side of Lake Constance with bio-optical conditions differing from the main water body, the differences between WASI-AI and WASI-2D are the highest for retrievals of Chl-a and TSM from the Landsat-9 image (see Figs. 5 and 6). This example from Lake Constance illustrates that a poor agreement between WASI-AI and WASI-2D results indicates a need to refine the parametrization of the physical models. All maps show very strong spatial correspondences between WASI-AI and WASI-2D for all fit parameters. All dynamic structures are

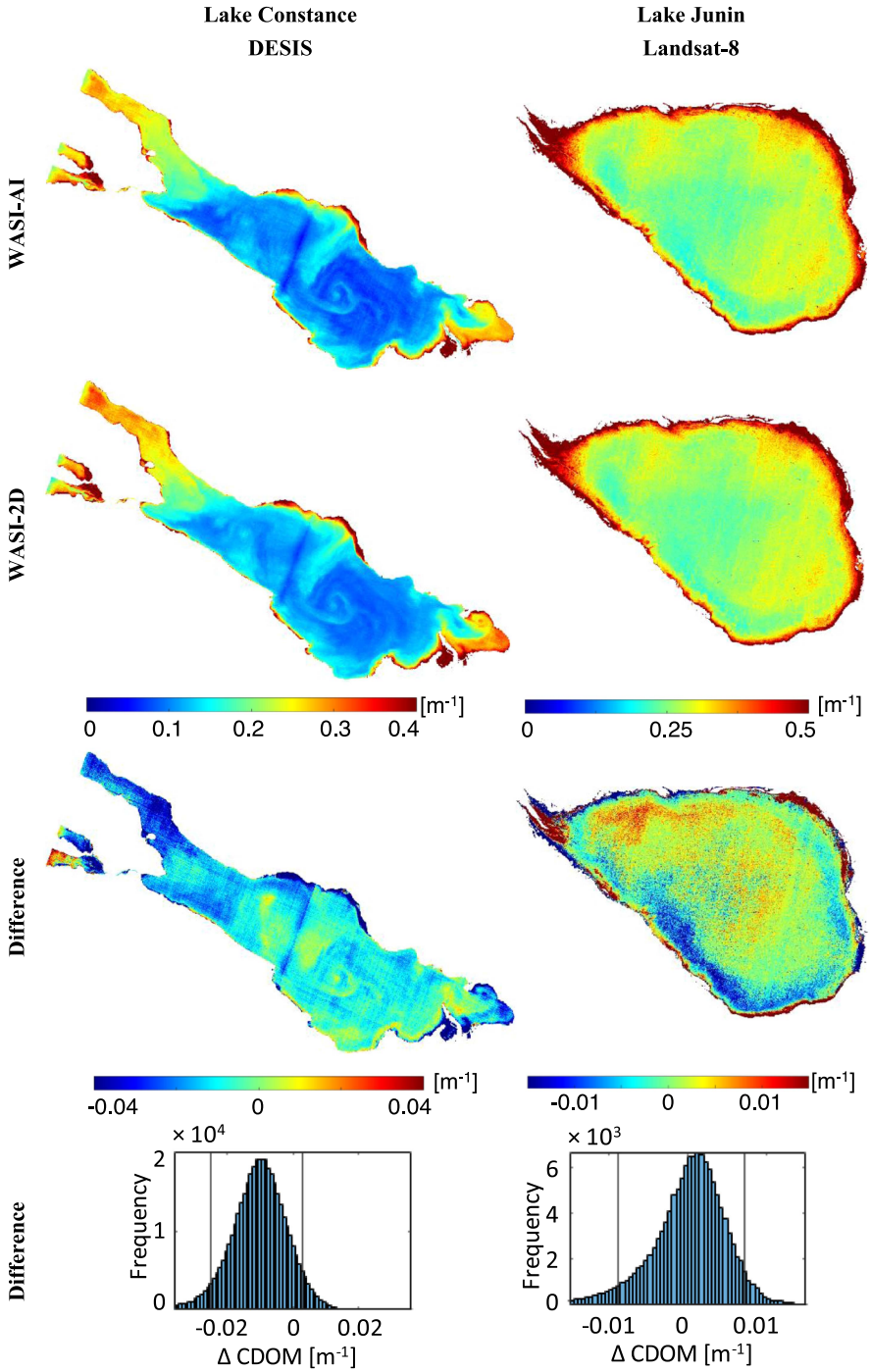

Fig. 7. CDOM maps derived from WASI-AI and WASI-2D, along with associated difference maps and histograms.

reproduced, even the highly variable sun glint patterns, which can differ strongly from pixel to pixel (see Fig. 8). Note that the strip effects on the DESIS maps (see Fig. 7) are related to the sensor noise.

C. Noise Reduction

The noise of all maps derived with WASI-AI is compared to that of WASI-2D using the RCV defined in Section II-C. The mean RCV values are less than one for all fit parameters (see Table IV), implying the advantage of WASI-AI in producing maps with less noise than WASI-2D. For instance, the Chl-a and TSM maps of WASI-AI are, on average, 12% and 13% less noisy than those of WASI-2D, respectively.

Fig. 10 compares the CV maps of WASI-AI and WASI-2D for the example of TSM retrieval in Lake Constance from the Landsat-9 image. The WASI-2D retrievals in the northern part of the lake exhibit high CV values, whereas the CV map of WASI-AI depicts low and homogeneous values across the lake, indicating reduced noise levels. This finding is also visually

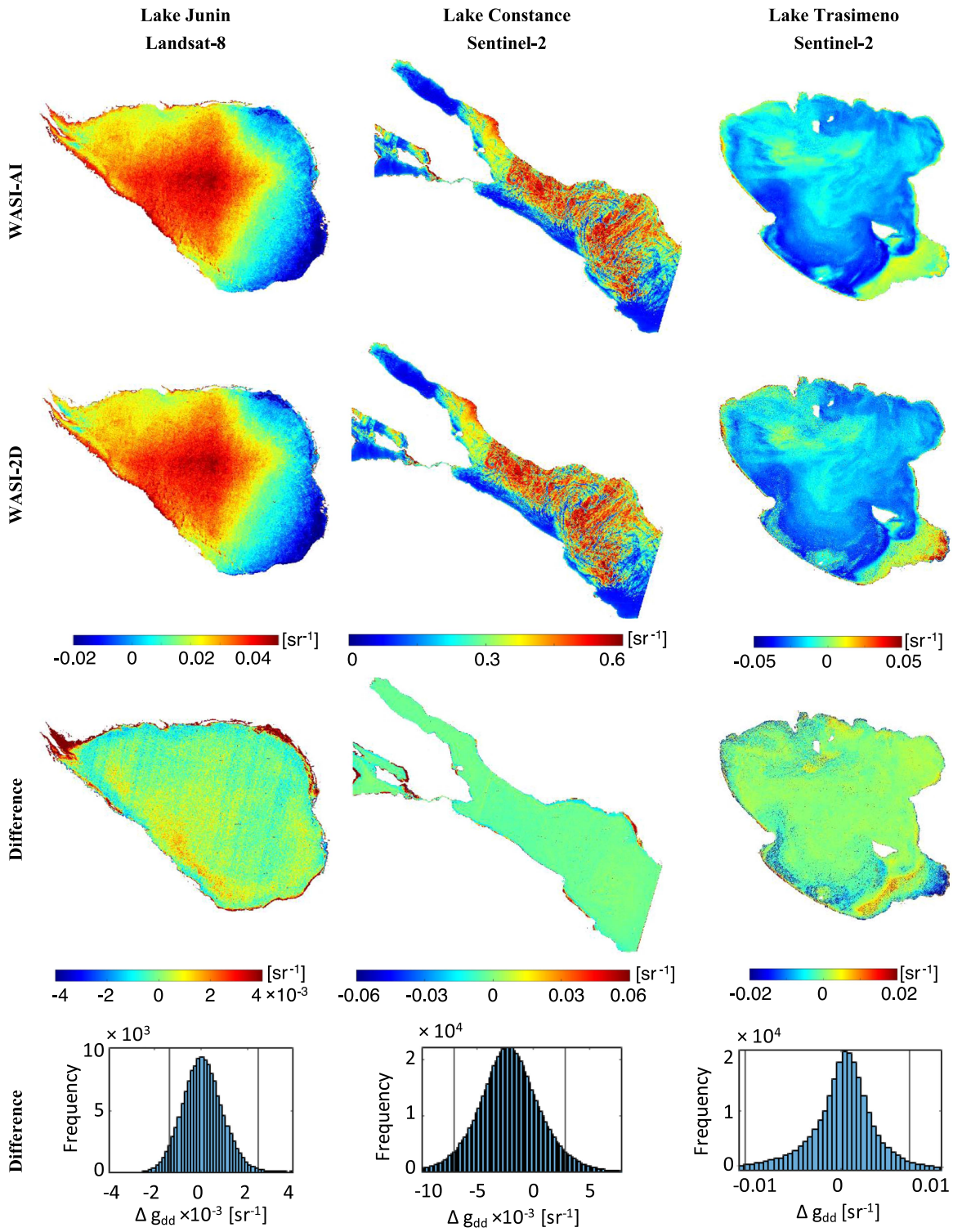

Fig. 8. g_{dd} maps derived from WASI-AI and WASI-2D, along with associated difference maps and histograms.

evident from the TSM maps (see Fig. 6), indicating noisy estimates in the northern part of the lake. An RCV of 0.66 is achieved for this map pair, corresponding to a significantly lower (34%) noise level for the WASI-AI map.

D. Reduction of Processing Time

Table V reports the processing times of WASI-AI and WASI-2D for different images. All images were processed on a computer with an Intel Xeon 3.8 GHz quad-core processor and 64 GB RAM. The WASI-2D processing takes up to ∼26 h in

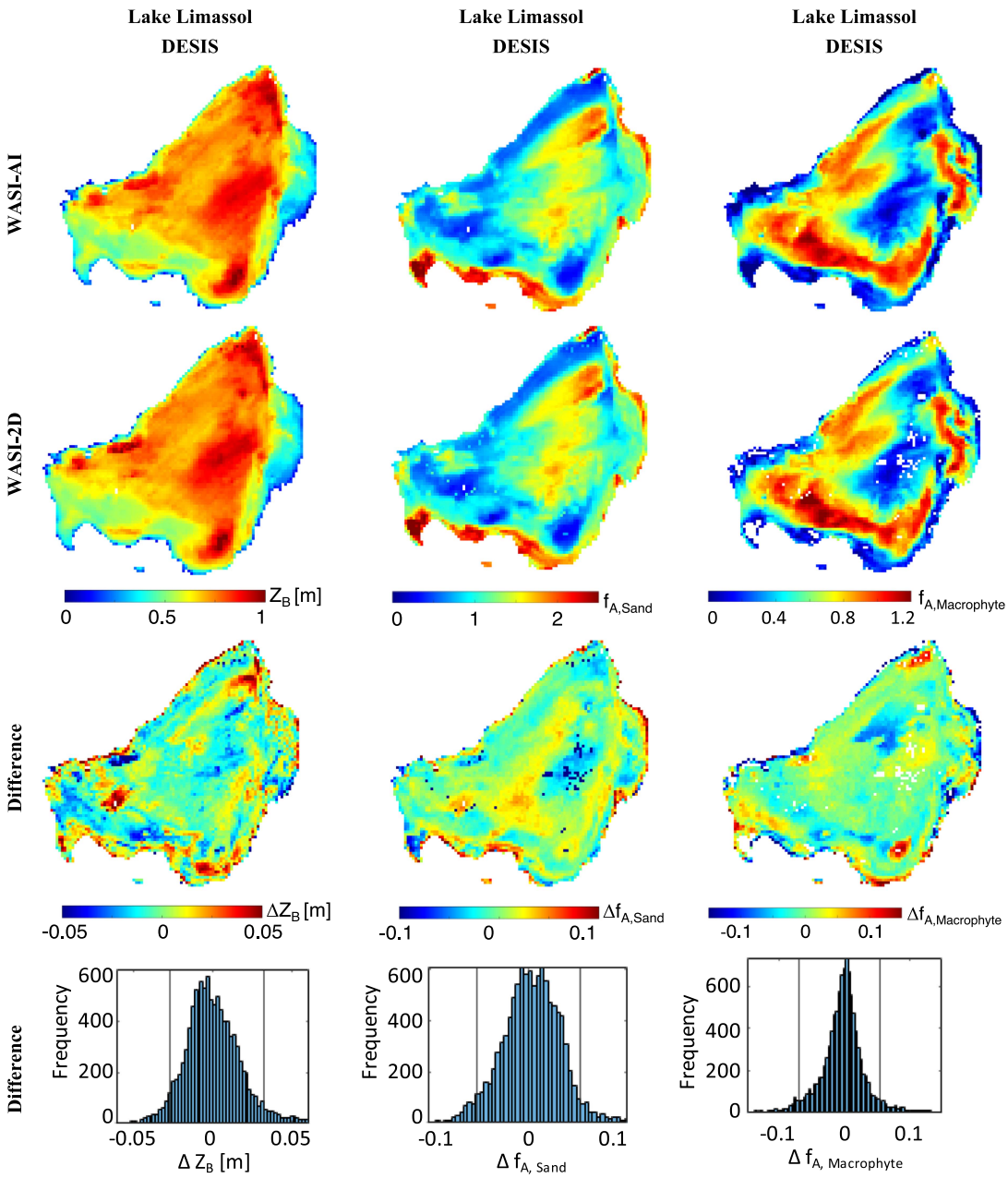

Fig. 9. Water depth and bottom brightness maps derived from WASI-AI and WASI-2D, along with associated difference maps and histograms.

the case of the Sentinel-2 image of Lake Constance, whereas it takes only ∼2 min for WASI-AI (749 times faster). As another example, WASI-AI is 1179 times faster than WASI-2D inverting the Sentinel-2 image of Lake Garda. Although the computational time of WASI-AI increases with the number of spectral bands, all images, whether multispectral or hyperspectral, are processed in under 3.5 min. WASI-2D takes approximately 4.7 days for all inversions, whereas WASI-AI reduces it to only about 19.5 min. These results demonstrate the significant advantage of using WASI-AI over the traditional WASI-2D in terms of faster and more efficient retrieval of water quality and benthic properties.

V. Discussion

The new WASI-AI method accelerates image processing by two to three orders of magnitude and provides feedback for the parametrization of physical models. The agreement analysis for the validation samples serves as an assessment of the suitability of the parametrization. A poor WASI-AI versus WASI-2D agreement for one or more fit parameters suggests that the parametrization requires tuning. Although a strong agreement between WASI-AI and WASI-2D results cannot guarantee high accuracy of the retrieved parameters due to the natural variability of optical properties, it ensures the unambiguousness of the inversion results as the two methods are based on independent

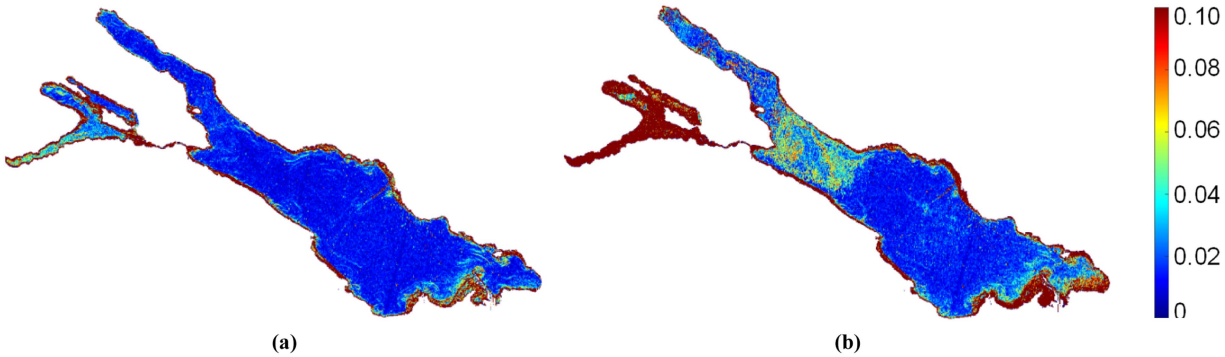

Fig. 10. Coefficient of variation (CV) of TSM maps derived from (a) WASI-AI and (b) WASI-2D processing Landsat-9 image in Lake Constance.

TABLE V
COMPARING THE PROCESSING TIME OF WASI-AI WITH WASI-2D

Water body	Water type	Image	WASI-AI [min]	WASI-2D [min]	Times faster
Amathus Harbour	Shallow	DESIS	2.9	81	28
Lake Constance	Deep	EnMAP	2.2	719	327
	Deep	DESIS	3.5	1183	338
	Deep	Landsat-9	1	774	774
	Deep	Sentinel-2	2.1	1572	749
Lake Garda	Deep	Sentinel-2	1	1179	1179
Lake Junin	Deep	Landsat-8	0.78	193	247
	Shallow		0.8	122	152
	Deep	Sentinel-2	1	355	355
	Shallow		0.7	88	125
Laguna Lasuntay	Deep	SuperDove	0.75	42	56
Lake Limassol	Shallow	DESIS	2	36	18
Lake Trasimeno	Deep	Sentinel-2	0.8	373	466

TABLE IV
NOISE LEVELS OF MAPS DERIVED FROM WASI-AI RELATIVE TO WASI-2D QUANTIFIED IN TERMS OF RCV FOR ALL FIT PARAMETERS

		C_{chl-a}	C_X	C_Y	z_B	f_A	g_{dd}
RCV	Range	0.41-1.02	0.66-1	0.98-1.03	0.87-1.01	0.73-1.03	0.32-1.03
	Mean	0.88	0.87	0.99	0.97	0.90	0.78
	SD	0.23	0.12	0.02	0.07	0.11	0.28

approaches. Traditionally, users had to manually evaluate WASI-2D's final maps after hours or even days of processing to identify unreliable fit parameters based on noisy outputs. This process required repeating the inversion with adjusted parameterization, making the procedure excessively time-consuming and limiting the practical usability of WASI-2D. Experimental results using various multi- and hyperspectral imagery demonstrated that WASI-AI inversion results strongly correspond to those of WASI-2D for different fit parameters after minimizing the ambiguities. Furthermore, the maps produced by WASI-AI exhibit lower noise than those of WASI-2D. WASI-AI significantly speeds up image inversion, making it invaluable for efficiently processing imagery across extensive spatial and temporal scales.

The samples inverted by WASI-2D are selected at random locations on the image to capture the variability of bio-optical conditions within the scene. If an inappropriate parametrization of WASI-2D results in high inversion residuals, a significant portion of the samples may be removed during the outlier removal stage. This reduction in the number of samples can be observed on the scatter plots. Consequently, the user can increase the number of samples and/or adjust the parametrization of WASI-2D to repeat the inversion process. The high residual values for certain samples indicate significant uncertainties in the WASI-2D inversion results for those samples, leading to their exclusion. Extraordinary bio-optical conditions, such as sediment plumes and algal blooms, can complicate image analysis. This complexity arises because a single parametrization of WASI-2D may not be suitable for processing an entire image with extensive bio-optical variability. Therefore, the image should be processed in multiple (usually two) steps, using different parametrizations of WASI-2D for regions with markedly different bio-optical conditions.

The adaptability of WASI-2D, and thus, WASI-AI, to diverse bio-optical environments enables it to effectively handle the complex conditions in aquatic systems. In contrast, existing NN-based algorithms such as C2RCC lack this flexibility and tend to perform poorly under challenging scenarios, particularly in the presence of algal scums or floating blooms [42]. This limitation stems from their reliance on extensive simulated training datasets, which are often constrained by substantial spectral ambiguities.

VI. CONCLUSION

The newly developed WASI-AI provides a framework for the synergistic integration of AI and physics for retrieving biophysical parameters in aquatic systems from multi- and hyperspectral imagery. The inversion using physical models benefits from WASI-AI versus WASI-2D correlation plots for the validation samples to identify ambiguity problems and, thus, optimize the parametrization. On the other hand, the AI component benefits from the training samples produced by the physical modeling to train NNs. This approach allows for creating training samples tailored to the specific bio-optical conditions of the given image by accounting for the underlying physics.

WASI-AI adapts the number of layers and neurons in the NN architectures according to the number of spectral bands that provided high performance in various experiments. In addition, advanced hyperparameter tuning can be employed, but it increases the computation time. Although the current NN architectures are efficient, the WASI-AI software module provides a tuning option based on Bayesian optimization [43] that is not used in this study.

The routine processing of imagery on large scales can significantly benefit from WASI-AI, given its high-speed processing, low noise level, and the feedback provided to the physics-based parametrization. The close integration of AI with physical modeling in the framework of WASI-AI opens up new opportunities in remote sensing of water quality and benthic properties. Although the proposed integration of AI with physics-based modeling is developed for the WASI software, it is generic and can be implemented in other similar physics-based models.

Software Availability

The developed AI method has been incorporated into the software WASI as a new module WASI-AI that allows the user to apply this new inversion approach for image analysis. The core of WASI-AI is implemented as a standalone MATLAB software and called by WASI. There is no need for MATLAB software or a license to be installed. The only requirement is to install MATLAB Runtime, which can be obtained freely from the MathWorks website: https://www.mathworks.com/products/compiler/matlab-runtime.html (accessed on 15 Jan., 2025).

Since MathWorks specifies that end users can run applications created by MATLAB compiler royalty-free using MATLAB Runtime (https://www.mathworks.com/products/compiler.html#encrypted-royalty-free), MathWorks bears the responsibility for all modules and components utilized by MATLAB Runtime and associated licensing issues. The user is referred to the WASI manual for information about the installation of MATLAB Runtime. WASI, including the WASI-2D and WASI-AI modules and the relevant manuals, is available at: www.ioccg.org/data/software.html.

Acknowledgment

Author M. Niroumand-Jadidi was funded with a DLR-DAAD Research Fellowship offered by the German Aerospace Center (DLR) and the German Academic Exchange Service (DAAD) to conduct research as a guest scientist at DLR for developing WASI-AI.

References

[1] J. C. Ritchie, P. V. Zimba, and J. H. Everitt, "Remote sensing techniques to assess water quality," *Photogrammetric Eng. Remote Sens.*, vol. 69, no. 6, pp. 695–704, Jun. 2003, doi: 10.14358/PERS.69.6.695.

[2] A. Pacheco, J. Horta, C. Loureiro, and O. Ferreira, "Retrieval of nearshore bathymetry from Landsat 8 images: A tool for coastal monitoring in shallow waters," *Remote Sens. Environ.*, vol. 159, pp. 102–116, Mar. 2015, doi: 10.1016/j.rse.2014.12.004.

[3] M. W. Matthews, "A current review of empirical procedures of remote sensing in Inland and near-coastal transitional waters," *Int. J. Remote Sens.*, vol. 32, no. 21, pp. 6855–6899, Nov. 2011, doi: 10.1080/01431161.2010.512947.

[4] M. A. Warren, S. G. H. Simis, and N. Selmes, "Complementary water quality observations from high and medium resolution Sentinel sensors by aligning chlorophyll-A and turbidity algorithms," *Remote Sens. Environ.*, vol. 265, 2021, Art. no. 112651, doi: 10.1016/j.rse.2021.112651.

[5] H. R. Gordon, D. K. Clark, J. L. Mueller, and W. A. Hovis, "Phytoplankton pigments from the Nimbus-7 coastal zone color scanner: Comparisons with surface measurements," *Sciince (1979)*, vol. 210, no. 4465, pp. 63–66, 1980, doi: 10.1126/science.210.4465.63.

[6] K. Toming, T. Kutser, A. Laas, M. Sepp, B. Paavel, and T. Nõges, "First experiences in mapping lake water quality parameters with Sentinel-2 MSI imagery," *Remote Sens. (Basel)*, vol. 8, no. 8, Aug. 2016, Art. no. 640, doi: 10.3390/rs8080640.

[7] M. Niroumand-Jadidi, F. Bovolo, M. Bresciani, P. Gege, and C. Giardino, "Water quality retrieval from Landsat-9 (OLI-2) imagery and comparison to Sentinel-2," *Remote Sens. (Basel)*, vol. 14, no. 18, 2022, Art. no. 4596, doi: 10.3390/rs14184596.

[8] M. Niroumand-Jadidi, C. J. Legleiter, and F. Bovolo, "River bathymetry retrieval from Landsat-9 images based on neural networks and comparison to super dove and Sentinel-2," *IEEE J. Sel. Top. Appl. Earth Obs. Remote Sens.*, vol. 15, pp. 5250–5260, 2022, doi: 10.1109/JSTARS.2022.3187179.

[9] D. Odermatt, A. Gitelson, V. E. Brando, and M. Schaepman, "Review of constituent retrieval in optically deep and complex waters from satellite imagery," *Remote Sens. Environ*, vol. 118, pp. 116–126, 2012, doi: 10.1016/j.rse.2011.11.013.

[10] B. Arabi, M. S. Salama, D. van der Wal, J. Pitarch, and W. Verhoef, "The impact of sea bottom effects on the retrieval of water constituent concentrations from MERIS and OLCI images in shallow tidal waters supported by radiative transfer modeling," *Remote Sens. Environ.*, vol. 237, 2020, Art. no. 111596, doi: 10.1016/j.rse.2019.111596.

[11] M. Defoin-Platel and M. Chami, "How ambiguous is the inverse problem of ocean color in coastal waters?," *J. Geophys Res.*, vol. 112, no. C3, Mar. 2007, Art. no. C03004, doi: 10.1029/2006JC003847.

[12] C. Giardino, V. E. Brando, A. G. Dekker, N. Strömbeck, and G. Candiani, "Assessment of water quality in Lake Garda (Italy) using Hyperion," *Remote Sens. Environ.*, vol. 109, no. 2, pp. 183–195, Jul. 2007, doi: 10.1016/J.RSE.2006.12.017.

[13] C. Niu, K. Tan, X. Wang, P. Du, and C. Pan, "A semi-analytical approach for estimating inland water inherent optical properties and chlorophyll a using airborne hyperspectral imagery," *Int. J. Appl. Earth Observation Geoinformation*, vol. 128, 2024, Art. no. 103774, doi: 10.1016/j.jag.2024.103774.

[14] M. Niroumand-Jadidi, F. Bovolo, and L. Bruzzone, "Water quality retrieval from PRISMA hyperspectral images: First experience in a Turbid Lake and comparison with Sentinel-2," *Remote Sens. (Basel)*, vol. 12, no. 23, Dec. 2020, Art. no. 3984, doi: 10.3390/rs12233984.

[15] M. Bresciani et al., "Application of new hyperspectral sensors in the remote sensing of aquatic ecosystem health: Exploiting PRISMA and DESIS for four Italian Lakes," *Resources*, vol. 11, no. 2, 2022, Art. no. 8, doi: 10.3390/resources11020008.

[16] M. Niroumand-Jadidi, A. Vitti, and D. R. Lyzenga, "Multiple optimal depth predictors analysis (MODPA) for river bathymetry: Findings from spectroradiometry, simulations, and satellite imagery," *Remote Sens. Environ.*, vol. 218, pp. 132–147, Dec. 2018, doi: 10.1016/j.rse.2018.09.022.

[17] M. Niroumand-Jadidi and F. Bovolo, "Temporally transferable machine learning model for total suspended matter retrieval from Sentinel-2," *ISPRS Ann. Photogrammetry, Remote Sens. Spatial Inf. Sci.*, vol. V-3–2022, pp. 339–345, 2022, doi: 10.5194/isprs-annals-V-3-2022-339-2022.

[18] Y. Sun, D. Wang, L. Li, R. Ning, S. Yu, and N. Gao, "Application of remote sensing technology in water quality monitoring: From traditional approaches to artificial intelligence," *Water Res.*, vol. 267, 2024, Art. no. 122546, doi: 10.1016/j.watres.2024.122546.

[19] C. Niu, K. Tan, X. Jia, and X. Wang, "Deep learning based regression for optically inactive inland water quality parameter estimation using airborne hyperspectral imagery," *Environ. Pollut.*, vol. 286, 2021, Art. no. 117534, doi: 10.1016/j.envpol.2021.117534.

[20] J. Pyo et al., "Long short-term memory models of water quality in inland water environments," *Water Res. X*, vol. 21, 2023, Art. no. 100207, doi: 10.1016/j.wroa.2023.100207.

[21] Y. Zhang, X. Kong, L. Deng, and Y. Liu, "Monitor water quality through retrieving water quality parameters from hyperspectral images using graph convolution network with superposition of multi-point effect: A case study in Maozhou River," *J. Environ. Manage*, vol. 342, 2023, Art. no. 118283, doi: 10.1016/j.jenvman.2023.118283.

[22] Z. Lee, K. L. Carder, C. D. Mobley, R. G. Steward, and J. S. Patch, "Hyperspectral remote sensing for shallow waters. 2. Deriving bottom depths and water properties by optimization," *Appl. Opt.*, vol. 38, no. 18, pp. 3831–3843, Jun. 1999.
[23] C. D. Mobley, *Light and Water : Radiative Transfer in Natural Waters*. New York, NY, USA: Academic, 1994.
[24] C. D. Mobley et al., "Interpretation of hyperspectral remote-sensing imagery by spectrum matching and look-up tables," *Appl. Opt.*, vol. 44, no. 17, pp. 3576–3592, Jun. 2005.
[25] C. Brockmann, R. Doerffer, M. Peters, K. Stelzer, S. Embacher, and A. Ruescas, "Evolution of the C2RCC neural network for Sentinel 2 and 3 for the retrieval of ocean colour products in normal and extreme optically complex waters," in *Proc. ESA Living Planet*, Prague, 2016, Art. no. 54.
[26] P. Gege, "WASI-2D: A software tool for regionally optimized analysis of imaging spectrometer data from deep and shallow waters," *Comput. Geosci.*, vol. 62, pp. 208–215, Jan. 2014, doi: 10.1016/J.CAGEO.2013.07.022.
[27] E. Politi, M. E. J. Cutler, and J. S. Rowan, "Evaluating the spatial transferability and temporal repeatability of remote-sensing-based lake water quality retrieval algorithms at the European scale: A meta-analysis approach," *Int. J. Remote Sens.*, vol. 36, no. 11, pp. 2995–3023, Jun. 2015, doi: 10.1080/01431161.2015.1054962.
[28] P. Gege, "The water color simulator WASI: An integrating software tool for analysis and simulation of optical in situ spectra," *Comput. Geosci.*, vol. 30, no. 5, pp. 523–532, Jun. 2004, doi: 10.1016/j.cageo.2004.03.005.
[29] C. Giardino, G. Candiani, M. Bresciani, Z. Lee, S. Gagliano, and M. Pepe, "BOMBER: A tool for estimating water quality and bottom properties from remote sensing images," *Comput. Geosci.*, vol. 45, pp. 313–318, Aug. 2012, doi: 10.1016/j.cageo.2011.11.022.
[30] P. Gege and A. Albert, "A tool for inverse modeling of spectral measurements in deep and shallow waters," in *Remote Sensing of Aquatic Coastal Ecosystem Processes*, L. L. Richardson and E. F. LeDrew, Eds. Dordrecht, The Netherlands: Springer, 2006, pp. 81–109, doi: 10.1007/1-4020-3968-9_4.
[31] A. Manuel, A. C. Blanco, A. M. Tamondong, R. Jalbuena, O. Cabrera, and P. Gege, "Optmization of BIO-Optical model parameters for Turbid Lake water quality estimation using landsat 8 and Wasi-2D," *ISPRS - Int. Arch. Photogrammetry, Remote Sens. Spatial Inf. Sci.*, vol. XLII-3/W11, pp. 67–72, Feb. 2020, doi: 10.5194/isprs-archives-xlii-3-w11-67-2020.
[32] M. Niroumand-Jadidi, F. Bovolo, L. Bruzzone, and P. Gege, "Inter-Comparison of methods for Chlorophyll-a Retrieval: Sentinel-2 Time-Series analysis in Italian Lakes," *Remote Sens (Basel)*, vol. 13, no. 12, Jun. 2021, Art. no. 2381, doi: 10.3390/rs13122381.
[33] E. Alevizos and D. D. Alexakis, "Monitoring Short-Term morphobathymetric change of nearshore seafloor using Drone-Based multispectral imagery," *Remote Sens. (Basel)*, vol. 14, no. 23, 2022, Art. no. 6035, doi: 10.3390/rs14236035.
[34] A. Göritz et al., "Retrieval of water constituents from Hyperspectral In-Situ measurements under variable cloud Cover—A case study at Lake Stechlin (Germany)," *Remote Sens. (Basel)*, vol. 10, no. 2, Jan. 2018, Art. no. 181, doi: 10.3390/rs10020181.
[35] C. Leys, C. Ley, O. Klein, P. Bernard, and L. Licata, "Detecting outliers: Do not use standard deviation around the mean, use absolute deviation around the median," *J. Exp. Soc. Psychol.*, vol. 49, no. 4, pp. 764–766, Jul. 2013, doi: 10.1016/j.jesp.2013.03.013.
[36] F. Murtagh, "Multilayer perceptrons for classification and regression," *Neurocomputing*, vol. 2, no. 5/6, pp. 183–197, Jul. 1991, doi: 10.1016/0925-2312(91)90023-5.
[37] A. K. Jain, J. Mao, and K. M. Mohiuddin, "Artificial neural networks: A tutorial," *Comput. (Long Beach Calif)*, vol. 29, no. 3, pp. 31–44, 1996, doi: 10.1109/2.485891.
[38] B. N. Seegers, R. P. Stumpf, B. A. Schaeffer, K. A. Loftin, and P. J. Werdell, "Performance metrics for the assessment of satellite data products: An ocean color case study," *Opt Exp.*, vol. 26, no. 6, pp. 7404–7422, Mar. 2018, doi: 10.1364/OE.26.007404.
[39] R. de los Reyes et al., "PACO: Python-Based atmospheric correction," *Sensors*, vol. 20, no. 5, 2020, Art. no. 1428, doi: 10.3390/s20051428.
[40] Q. Vanhellemont, "Sensitivity analysis of the dark spectrum fitting atmospheric correction for metre- and decametre-scale satellite imagery using autonomous hyperspectral radiometry," *Opt. Exp.*, vol. 28, no. 20, pp. 29948–29965, Sep. 2020, doi: 10.1364/OE.397456.
[41] P. Gege, "A spectral weighting function for improving phytoplankton classification," in *Proc. HISE*, Munich, 2023, pp. 1–2, doi: 10.1364/HMISE.2023.HW4C.2.
[42] K. Xue, R. Ma, H. Duan, M. Shen, E. Boss, and Z. Cao, "Inversion of inherent optical properties in optically complex waters using sentinel-3A/OLCI images: A case study using China's three largest Freshwater Lakes," *Remote Sens. Environ.*, vol. 225, pp. 328–346, 2019, doi: 10.1016/j.rse.2019.03.006.
[43] J. Snoek, H. Larochelle, and R. P. Adams, "Practical bayesian optimization of machine learning algorithms," in *Advances in Neural Information Processing Systems*, F. Pereira, C. J. Burges, L. Bottou, and K. Q. Weinberger, Eds., New York, NY, USA: Curran Associates, 2012.

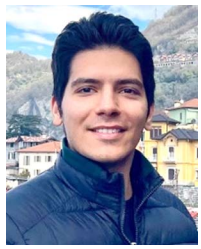

Milad Niroumand-Jadidi (Member, IEEE) received the B.Sc. degree in geomatics engineering from the University of Tabriz, Tabriz, Iran, in 2009, the M.Sc. degree in remote sensing engineering from K.N. Toosi University of Technology, Tehran, Iran, in 2013, and the joint Ph.D. degree in civil and environmental engineering from the University of Trento, Trento, Italy and from Freie Universität Berlin, Berlin, Germany, in 2017.

From 2017 to 2024, he has been a Postdoctoral Researcher with the Remote Sensing for Digital Earth unit of the Digital Society Center at Fondazione Bruno Kessler, Trento, Italy. He is currently a Researcher with the Interdepartmental Research Centre for Environmental Sciences, University of Bologna, Bologna, Italy. He has authored and coauthored more than 20 peer-reviewed articles in top journals and presented numerous papers at international conferences. His main research interests include the development of methods and applications for remote sensing of inland and coastal waters from optical data

Dr. Niroumand-Jadidi was the recipient of several international awards, recipient of a DLR-DAAD fellowship for spending three months (May−Aug. 2022) as a visiting scientist with the German Aerospace Center, the recipient of Best Young Author Award from the International Society for Photogrammetry and Remote Sensing in 2021, recipient of the best paper award from SPIE Remote Sensing conferences for three years in a row (2015 in Toulouse, 2016 in Edinburgh, and 2017 in Warsaw), the recipient of the award for potential long-range contribution to the field of optics and photonics from SPIE (The international society for optics and photonics) in 2016, and the recipient of Alexander Goetz Instrument Support Award 2016, which gave him access to a field spectroradiometer during his Ph.D. research.

He focuses on both physics-based and machine learning models to retrieve information on water quality and bathymetry. He serves on the editorial board for the journal Remote Sensing and has also been a special issue editor. He is a referee for several international journals, including IEEE TRANSACTIONS ON GEOSCIENCE AND REMOTE SENSING, IEEE JOURNAL OF SELECTED TOPICS IN APPLIED EARTH OBSERVATIONS AND REMOTE SENSING, *Remote Sensing of Environment*, *Remote Sensing*, *Journal of Hydrology*, *Water, and International Journal of Remote Sensing*.

Peter Gege received the Diploma in physics from the Technical University of Munich, Munich, Germany, in 1988 and the Ph.D. degree in natural sciences from the University of Hamburg, Hamburg, Germany, in 1994.

He is leading the team Aquatic Remote Sensing with the Remote Sensing Technology Institute of the German Aerospace Center, Oberpfaffenhofen, Germany. He has 35 years of experience in hyperspectral remote sensing and algorithm development for coastal and inland waters. He has authored and coauthored more than 50 articles in top peer-reviewed journals and books, and has presented his work at numerous international conferences. He has organized a number of national and international workshops, training courses, and field campaigns in aquatic remote sensing, and has participated in more than 20 projects. He developed the software tool water color simulator for the simulation and data analysis of spectral measurements in deep and shallow waters. He was responsible for establishing an ISO-certified optical laboratory for the calibration of airborne hyperspectral sensors. His research interests include radiative transfer modeling in water and the atmosphere, algorithm development for optically complex water types (inland, coastal, shallow), inverse modeling, calibration of field spectrometers and hyperspectral sensors, quality control, image processing, and data analysis of spectral measurements from satellite, aircraft, and ship.